© 2020. Published by The Company of Biologists Ltd | Journal of Cell Science (2020) 133, jcs235846. doi:10.1242/jcs.235846

SHORT REPORT

F-BAR domain protein Syndapin regulates actomyosin dynamics during apical cap remodeling in syncytial *Drosophila* embryos

Aparna Sherlekar*, Gayatri Mundhe[‡,¶], Prachi Richa[§,¶], Bipasha Dey, Swati Sharma and Richa Rikhy**

ABSTRACT

Branched actin networks driven by Arp2/3 interact with actomyosin filaments in processes such as cell migration. Similar interactions occur in the syncytial *Drosophila* blastoderm embryo where expansion of apical caps by Arp2/3-driven actin polymerization occurs in interphase, and cap buckling at contact edges by Myosin II to form furrows takes place in metaphase. Here, we study the role of Syndapin (Synd), an F-BAR domain-containing protein, in apical cap remodeling prior to furrow extension. We found that depletion of *synd* resulted in larger apical caps. Super-resolution and TIRF microscopy showed that control embryos had long apical actin protrusions in caps during interphase and short protrusions during metaphase, whereas *synd* depletion led to formation of sustained long protrusions, even during metaphase. Loss of Arp2/3 function in *synd* mutants partly reverted defects in apical cap expansion and protrusion remodeling. Myosin II levels were decreased in *synd* mutants, an observation consistent with the expanded cap phenotype previously reported for Myosin II mutant embryos. We propose that Synd function limits branching activity during cap expansion and affects Myosin II distribution in order to bring about a transition in actin remodeling activity from apical cap expansion to lateral furrow extension.

KEY WORDS: Actomyosin, Syndapin, Cap, Metaphase furrow, *Drosophila*

INTRODUCTION

Branched and bundled actin networks, along with contractile proteins, mediate processes such as cell migration and cell shape remodeling in embryogenesis. Directional motility in crawling cells is characterized by Arp2/3-driven branched actin polymerization at the leading edge of the lamellipodial sheet and by actomyosin-driven contractile forces in the lamella (Pollard and Borisy, 2003; Ponti et al., 2004). Apical actin rings in 16-cell-stage mouse embryos expand through polymerization by formins and trigger zippering of junctions at edges where they contact actomyosin (Zenker et al., 2018). Apical actin caps in *Drosophila* syncytial blastoderm embryos (Karr and Alberts, 1986) also expand, as a result of Arp2/3 complex activity, and meet at actomyosin borders to form lateral furrows with distinct polarity (Mavrakis et al., 2009; Schmidt and Grosshans, 2018; Zenker et al., 2018; Zhang et al., 2018). BAR domain-containing proteins are known to play a role in actin remodeling (Carman and Dominguez, 2018; Sherlekar and Rikhy, 2016; Stanishneva-Konovalova et al., 2016). The F-BAR domain-containing protein Syndapin (Synd) interacts with N-WASP via its SRC homology 3 (SH3) domain, thereby activating Arp2/3-mediated actin polymerization (Modregger, 2000; Kessels and Qualmann, 2002; Dharmalingam et al., 2009). However, its function in regulating transitions between different actin networks has not been studied. Here, we analyze the role of Synd in Arp2/3 complex- and actomyosin-driven actin cap remodeling in *Drosophila* syncytial blastoderm embryos.

The *Drosophila* syncytial embryo consists of cortical nuclei surrounded by an apical actomyosin-rich cap with microvilli (protrusions) that resemble filopodia (Foe and Alberts, 1983; Karr and Alberts, 1986; Mavrakis et al., 2009; Turner and Mahowald, 1976; Warn et al., 1980, 1984; Young et al., 1991). Apical caps expand during each nuclear cycle (NC) and come into contact with each other at sites where lateral furrows then extend between adjacent nuclei. Arp2/3 complex mutants have smaller apical caps, whereas Rho-kinase inhibition leading to loss of Myosin II results in larger caps (Cao et al., 2010; Stevenson et al., 2002; Zallen et al., 2002; Zhang et al., 2018). Expanding caps formed by cortical actomyosin assembly are also enriched in Anillin, Syndapin, the septin Peanut and the formin Diaphanous. Mutant embryos in which these proteins are disrupted show decreased furrow extension (Afshar et al., 2000; Fares et al., 1995; Field and Alberts, 1995; Foe et al., 2000; Sherlekar and Rikhy, 2016; Silverman-Gavrila et al., 2008).

Syndapin mutants show defects in recruitment of Peanut to the furrow (Sherlekar and Rikhy, 2016). The Anillin–Peanut complex compensates for Myosin II loss, favoring the transition of F-actin from the cap to the furrow and promoting furrow ingression (Zhang et al., 2018). We therefore performed an analysis of Syndapin function in regulating actin remodeling during cap expansion and furrow extension. Using a combination of live imaging by TIRF microscopy (TIRFM) and stimulated emission depletion (STED) microscopy, we show that interphase caps contain longer F-actin protrusions compared to metaphase caps. We find that *synd* mutants contain larger caps and sustained protrusions with increased F-actin remodeling and Arp2/3 activity. Syndapin function limits Arp2/3 activity during cap expansion to facilitate buckling by Myosin II for furrow extension.

RESULTS AND DISCUSSION

Syndapin mutant embryos contain enlarged caps, short furrows and defects in F-actin dynamics

We expressed a GFP-tagged version of the PH domain of GRP1 (tGPH, also known as Step), which binds the phospholipid phosphatidylinositol (3,4,5)-trisphosphate (Britton et al., 2002), in control and *synd* mutants to visualize apical cap area and furrow length dynamics during NC12 (Fig. 1A; Movie 1). Apical caps

Biology, Indian Institute of Science Education and Research, Homi Bhabha Road, Pashan, Pune 411008, India.
*Present address: Department of Molecular and Cellular Physiology, Stanford University School of Medicine, Stanford, CA 94305, USA. [‡]Present address: IBDM, 13009 Marseille Cedex 9, France. [§]Present address: Universitätsmedizin Göttingen, 37077 Göttingen, Lower Saxony, Germany. [¶]These authors contributed equally to this work

**Author for correspondence (richa@iiserpune.ac.in)

A.S., 0000-0003-3413-9599; R.R., 0000-0002-4262-0238

Handling Editor: David Glover
Received 11 July 2019; Accepted 6 April 2020

Journal of Cell Science (2020) 133, jcs235846. doi:10.1242/jcs.235846

expanded from interphase to prophase, contacted each other and lateral furrow extension occurred at the edges (Fig. 1B–D). Cap area increased in tGPH/+ embryos (Movie 1) until ∼6 min, after which the membranes came into contact and the area plateaued (∼6.5 min) while the lateral furrows continued to extend (Fig. 1D). We visualized F-actin dynamics during cap expansion in apical sections of embryos labeled with LifeAct–GFP (Fig. 1E). LifeAct–GFP levels increased at the cap periphery as they expanded but started to decrease once the caps were in contact (Fig. 1E,F). Depletion of the Arp3 subunit of the Arp2/3 complex resulted in significantly smaller caps that formed but did not expand and did not initiate lateral furrow formation (Fig. S1A–C, Movie 2). LifeAct–GFP failed to accumulate at the cap periphery in *arp3* mutants (Fig. S1D,E).

To test the role of Syndapin in cap and furrow dynamics, we used embryos from a previously reported hypomorphic allele of Syndapin in combination with a deficiency ($synd^{1d}$/Df, hereafter termed *synd*) (Kumar et al., 2009b; Sherlekar and Rikhy, 2016). Interestingly, on Syndapin depletion, caps were significantly larger and adjacent caps were already in contact in interphase (at 0 min). Cap expansion in *synd* reached a steady state earlier (∼4.5 min) than in controls (∼6.5 min) (Fig. 1B,C; Movie 3). Furrows were shorter in *synd* compared to those in controls (Fig. 1D). LifeAct–GFP localization increased at the cap periphery similar to controls (0-4 min) but remained at a significantly higher level in *synd*, even after the caps came into contact (>4 min) (Fig. 1E,F). The nuclear signal was visible in *synd* and not in controls, suggesting that the caps were flatter in *synd* (Fig. 1E). Syndapin function is likely to be important for limiting cap expansion and regulating F-actin dynamics at the cap periphery for the transition to furrow formation.

Syndapin mutants show sustained F-actin protrusions in apical caps

Scanning electron microscopy and TIRFM have shown protrusions in the apical domain of caps in interphase of the NC (Turner and Mahowald, 1976; Webb et al., 2009). To investigate the dynamics of actin-rich protrusions we observed the apical region of LifeAct–GFP-labeled caps using TIRFM and phalloidin-labeled F-actin structures using STED microscopy. In TIRFM, an evanescent excitation wave is propagated at the interface between two materials with different refractive indices and this results in the excitation of fluorophores within ∼100 nm of the interface (Axelrod, 2001). In LifeAct–GFP-expressing embryos, this wave illuminated the apical region of the cap. In control embryos, we saw apical villi-like protrusions (Fig. 2A), as previously observed in syncytial embryos using TIRFM (Webb et al., 2009). The protrusions appeared as puncta in the middle of the cap and were longer at the edge of the interphase cap, reflecting different orientations, similar to those observed apically by TIRFM during cellularization (Figard et al., 2016). In contrast, shorter protrusions in the form of puncta were observed throughout the metaphase cap. Only optically separable protrusions were used to quantify their observable length (Fig. S1F). The average protrusion length was 0.86 µm in interphase, and a few protrusions at the periphery were as long as ∼2.6 µm. The protrusions were significantly longer in interphase as compared to their length in metaphase where the average was 0.67 µm with a maximum of ∼1.5 µm (Fig. 2B). This suggested that long villi-like protrusions at the apical cap are remodeled at the time of furrow ingression.

STED super-resolution microscopy showed phalloidin-labeled, F-actin-containing protrusions at the cap periphery in control embryos. Apical structures in the form of puncta seen in TIRFM were not visible with phalloidin labeling in STED (Fig. S1F,G). Furthermore, in control metaphase caps protrusions were significantly shorter or absent, and F-actin was organized at cap edges along the depth of the furrow (Fig. 2C,D). In summary, the periphery of the interphase caps showed longer actin-rich protrusions, and this distribution was coincident with neighboring cap membranes approaching each other. Shorter protrusions were seen in metaphase when actin was enriched at the furrow (Fig. 2E).

In Arp3-depleted embryos, the majority of protrusions in interphase and metaphase caps were significantly shorter than controls (Fig. 2B) and were of similar length in interphase (average of 0.57 µm) and metaphase (average of 0.55 µm) (Fig. S1H,I). Thus, formation of long protrusions is Arp2/3 dependent, and their absence may result in loss of cap expansion (Stevenson et al., 2002; Zhang et al., 2018) (Fig. 2E, Fig. S1J).

In *synd*, the mean protrusion lengths in interphase (0.81 µm) and metaphase (0.75 µm) caps were not significantly different from each other and from the mean length in control interphase caps (Fig. 2A,B). The lack of a significant difference was also seen in phalloidin-labeled caps imaged with STED (Fig. 2C,D). Because protrusions remained long during metaphase in *synd*, we tested whether Arp2/3 localization was affected in *synd* mutants. In controls, Arp3 was enriched around the rim of the apical actin cap. In *synd*, Arp3 was spread across the entire cap surface (Fig. S2A), however, Arp3 levels were unchanged in interphase as compared to levels in controls (Fig. S2B).

We also performed fluorescence loss in photobleaching (FLIP) experiments using LifeAct–GFP to assess actin dynamics across the cap in control and *synd* embryos. LifeAct–GFP exchange during cap expansion was significantly faster in *synd* than in controls (Fig. S3A–D) suggesting an increase in F-actin remodeling across the apical domain. The spread of Arp3 localization throughout the cap in *synd* correlated with higher F-actin remodeling and may contribute to cap expansion and protrusion remodeling.

ArpC1 depletion in *synd* rescues apical cap expansion dynamics and furrow length

Vertebrate syndapins interact with N-WASP and activate Arp2/3-mediated actin polymerization (Modregger, 2000; Kessels and Qualmann, 2002). However, our data shows that depletion of Syndapin and Arp3 do not phenocopy each other. Syndapin mutants had larger caps, whereas Arp3 mutant caps failed to expand. This indicates that Syndapin and the Arp2/3 complex do not function in a linear pathway. To further confirm this, we depleted ArpC1, an essential component of the Arp2/3 complex, in the *synd* mutant background (*arp*C1/+; *synd*) and observed cap expansion and furrow extension using tGPH. Interestingly, we found that *arp*C1/+; *synd* had smaller caps (Fig. 3A,B) as compared to *synd* (Fig. 1C; Movie 4). In addition to this partial rescue of the cap size, furrow extension was also rescued (Fig. 3C). LifeAct–GFP accumulated at the cap periphery in *arp*C1/+; *synd* even though it remained at a lower level than in control embryos (Fig. S1D,E).

TIRFM revealed longer protrusions during interphase and shorter protrusions during metaphase in *arpC*1/+; *synd* (Fig. 3D,E) similar to the situation in control caps and unlike the protrusions observed for *synd* (Fig. 2A,B). Measurements of protrusion lengths in *arpC*1/+; *synd* revealed an average length of 0.72 µm in interphase (with a few protrusions reaching 2.4 µm) and 0.6 µm in metaphase (Fig. 3E). This significant difference in protrusion lengths between interphase and metaphase caps that reducing Arp2/3 complex activity in *synd* mutants allowed F-actin remodeling from long protrusions to short protrusions to occur during cap expansion and lateral furrow extension as the embryos progressed from interphase to metaphase. STED microscopy also revealed that,

Journal of Cell Science (2020) 133, jcs235846. doi:10.1242/jcs.235846

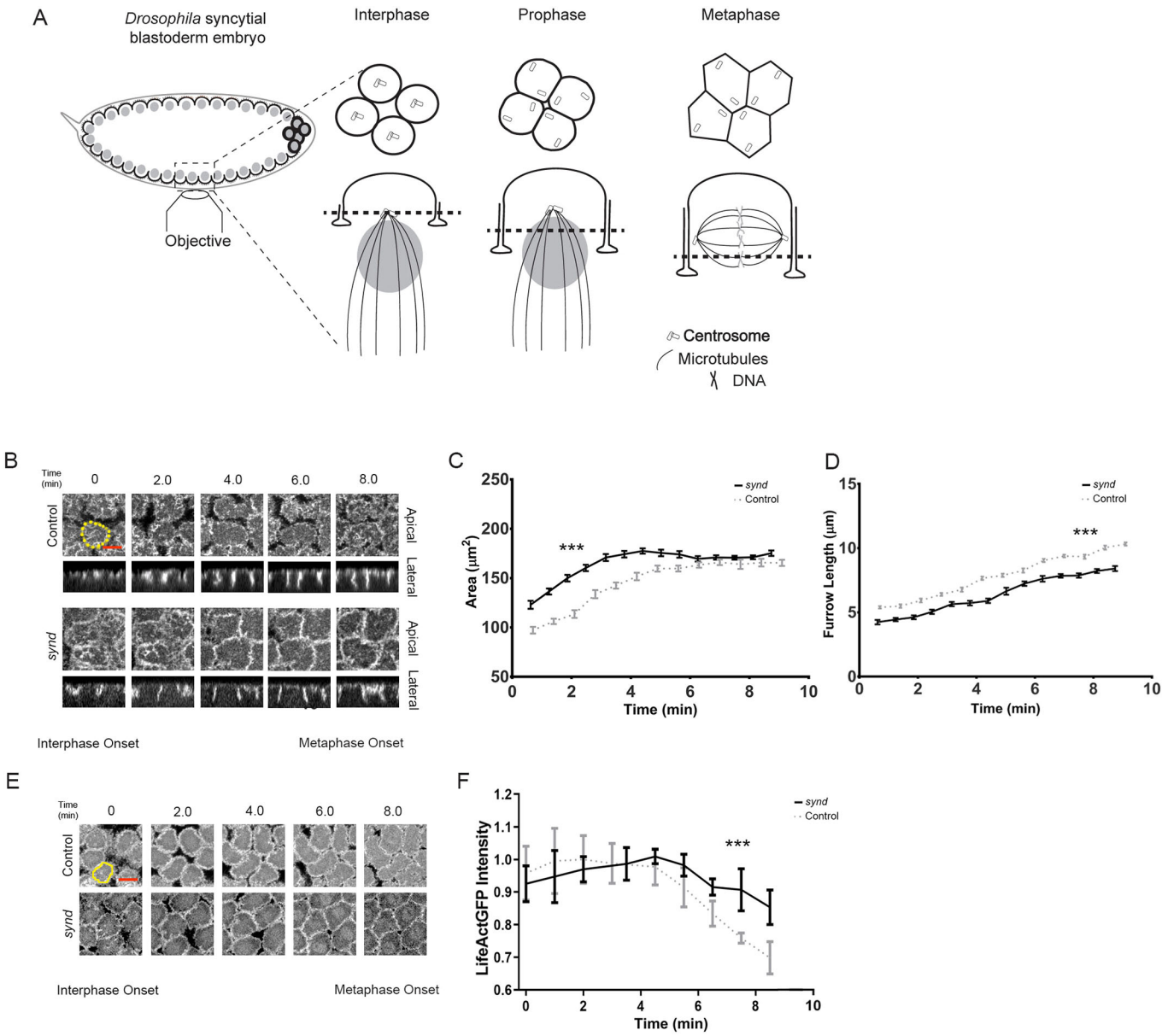

Fig. 1. *synd* shows defects in cap and furrow remodeling and F-actin dynamics. (A) Imaging *Drosophila* syncytial NCs using an inverted microscope (left). NC schematic (right) is rotated by 180° with apical at the top to represent the orientation in sagittal views. Interphase embryos have apical centrioles and short furrows, and metaphase embryos have lateral centrosomes and long furrows. Dashed line indicates the plane of membrane shown in the top panel. (B–D) *synd* embryos expressing tGPH show significantly increased NC12 cap area (B,C) and significantly shorter furrow length (B,D). (E,F) Peripheral LifeAct–GFP intensity in *synd* embryos is significantly higher than in controls. Graphs show mean±s.e.m. for n=3 embryos, with three caps quantified per embryo. ***P=0.001 (one-way ANOVA and Tukey's multiple comparison test). Scale bars: 10 µm.

unlike in *synd* embryos (Fig. 2C,D), long F-actin protrusions were not seen during metaphase of *arp*C1/+; *synd* embryos, an observation consistent with the rescue of cap expansion and furrow extension (Fig. 3F,G). The rescue of cap expansion and furrow extension in *arp*C1/+; *synd* also suggested that these embryos were able to remodel their protrusions to transition from cap expansion to furrow ingression (Fig. 3H).

Myosin II is reduced at the cortex and remains associated with the metaphase furrow membrane in *synd* mutants

Non-muscle Myosin II is implicated in restricting cap expansion, driving buckling at cap edges during the transition to furrow formation and creating tension across the cap (Sommi et al., 2011; Zhang et al., 2018). We used an anti-Zipper (Myosin II heavy chain) antibody and Sqh–GFP (Myosin II light chain reporter) to observe the Myosin II distribution in fixed and live samples of control and *synd* embryos. Zipper and Sqh–GFP (Fig. 4A,B) displayed distinct dynamic localization during the NC compared to the localization of the membrane marker Dlg; they localized to the cap periphery during expansion, and were cytosolic at metaphase with enrichment in the spindle region when the lateral furrows were at their longest (Royou et al., 2002). Zipper staining was reduced overall and was not present in the spindle region in *synd*. Zipper continued to be localized at vertices in metaphase – the points of highest tension in

Journal of Cell Science (2020) 133, jcs235846. doi:10.1242/jcs.235846

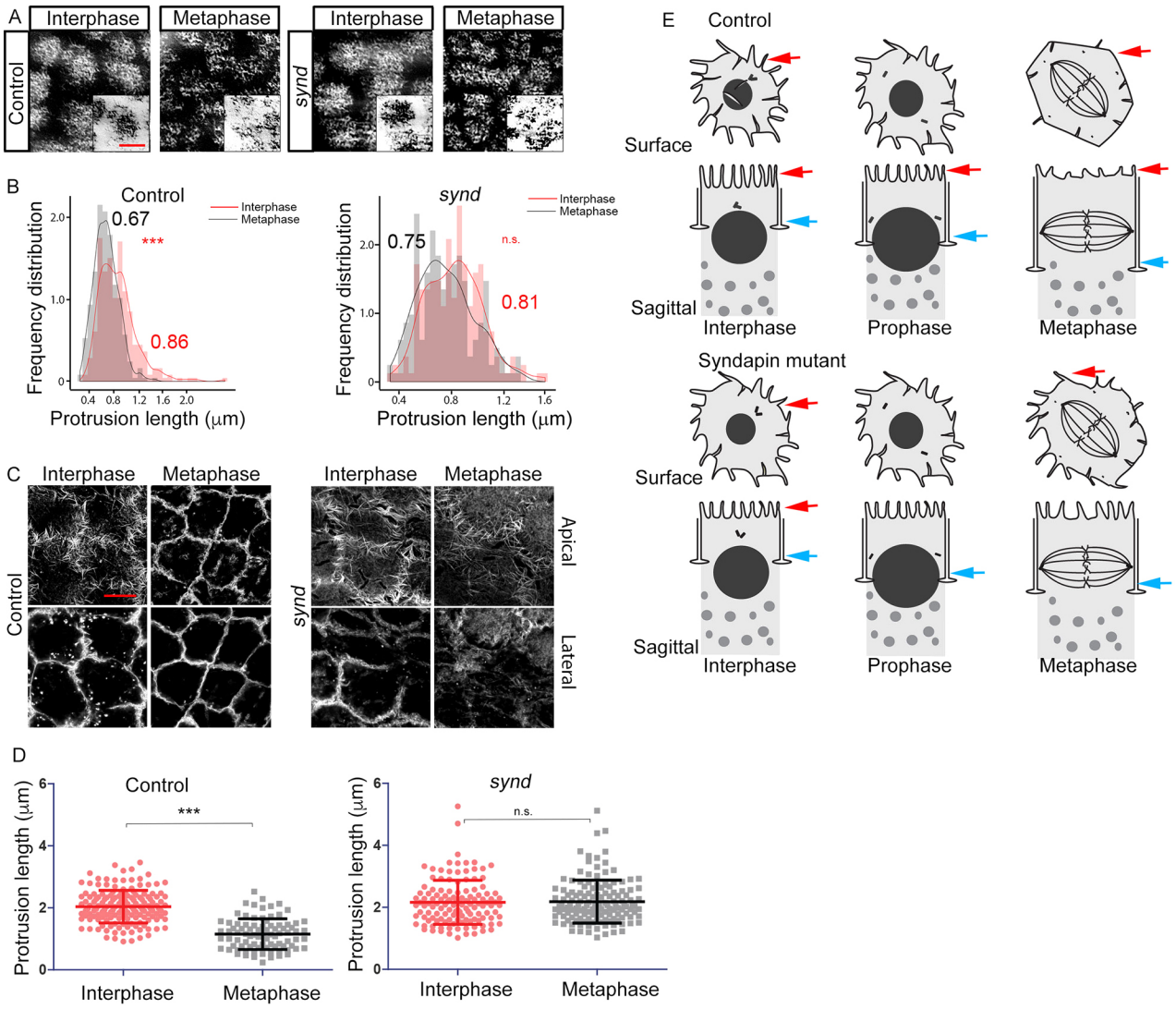

Fig. 2. Apical protrusion remodeling is defective in *synd*. (A) LifeAct–GFP-labeled protrusions in caps in control and *synd* NC12 embryos by TIRFM. Scale bar: 5 µm. (B) Relative frequency distributions of protrusion lengths show significantly longer interphase protrusions (0.86±0.3 µm, mean±s.d.) compared to metaphase protrusions (0.67±0.19 µm) in controls (***P<0.001) but not in *synd* (0.81±0.21 µm, interphase; 0.75±0.21 µm, metaphase; ns, P>0.05). n=100 protrusions per cap, three caps per embryo for three embryos. Statistical significance was tested using a one-way ANOVA and Tukey's multiple comparis on test. (C,D) STED microscopy of phalloidin-stained caps and furrows in control and *synd* NC12 embryos. Representative images are shown in C. Longer protrusions are observed during interphase and not during metaphase for control embryos. Long protrusions are present during metaphase and furrows are missing in 100% of *synd* embryos (n=10 embryos each). Protrusion lengths (mean±s.d.) are significantly different between interphase and metaphase for control embryos but not for *synd* embryos (D). n=3 embryos, ~50 protrusions/embryo. ***P<0.001; ns, P≥0.05 (two-tailed Mann–Whitney test). Scale bar: 3 µm. (E) Cap area increases and protrusion (red arrow) lengths decrease from interphase to metaphase in controls. In *synd*, the cap area is larger during interphase, apical protrusions remain and furrow length (blue arrow) is shorter than in controls during metaphase.

the cell membrane (Higashi and Miller, 2017) (Fig. 4A). Sqh–GFP intensities in the caps were also significantly lower in *synd* compared to intensities in controls (Fig. 4B,D; Movies 5–7), and Sqh–GFP remained on the membrane well after metaphase onset in *synd* mutant embryos (Fig. 4B,C). Sqh–GFP intensity remained low in *arp*C1/+; *synd* embryos but was lost from the furrow membrane in metaphase, similar to the Sqh–GFP dynamics observed in controls (Fig. 4B–D).

Cap and furrow dynamics were observed in sqh^{RNAi} embryos using tGPH. We observed that sqh^{RNAi} embryos phenocopied *synd* mutants; the cap area was larger, and furrow lengths significantly shorter, than in controls (Fig. S4A–C, Movie 8). In sqh^{RNAi} embryos, Syndapin levels were reduced on the membrane, with some Syndapin remaining at the vertices (Fig. S2A), and Arp3 was present on the membrane. Thus, the expanded caps in *synd* showed decreased Myosin II intensity (Fig. 4D) despite a small amount of Myosin II being retained on the metaphase membrane.

Our work can be summarized in a model where we predict that actin-rich apical protrusions in interphase retract into the cortex to supplement membrane and/or actin for furrow extension during metaphase. The growth of these long protrusions is dependent on activity of the Arp2/3 complex. Syndapin restricts Arp2/3 complex activity in cap expansion thereby supporting furrow extension in a timely manner. Once the caps come into contact, these protrusions are remodeled to drive furrow formation by buckling forces regulated by Myosin II contractile activity (Zhang et al., 2018), a transition step that requires Syndapin.

Journal of Cell Science (2020) 133, jcs235846. doi:10.1242/jcs.235846

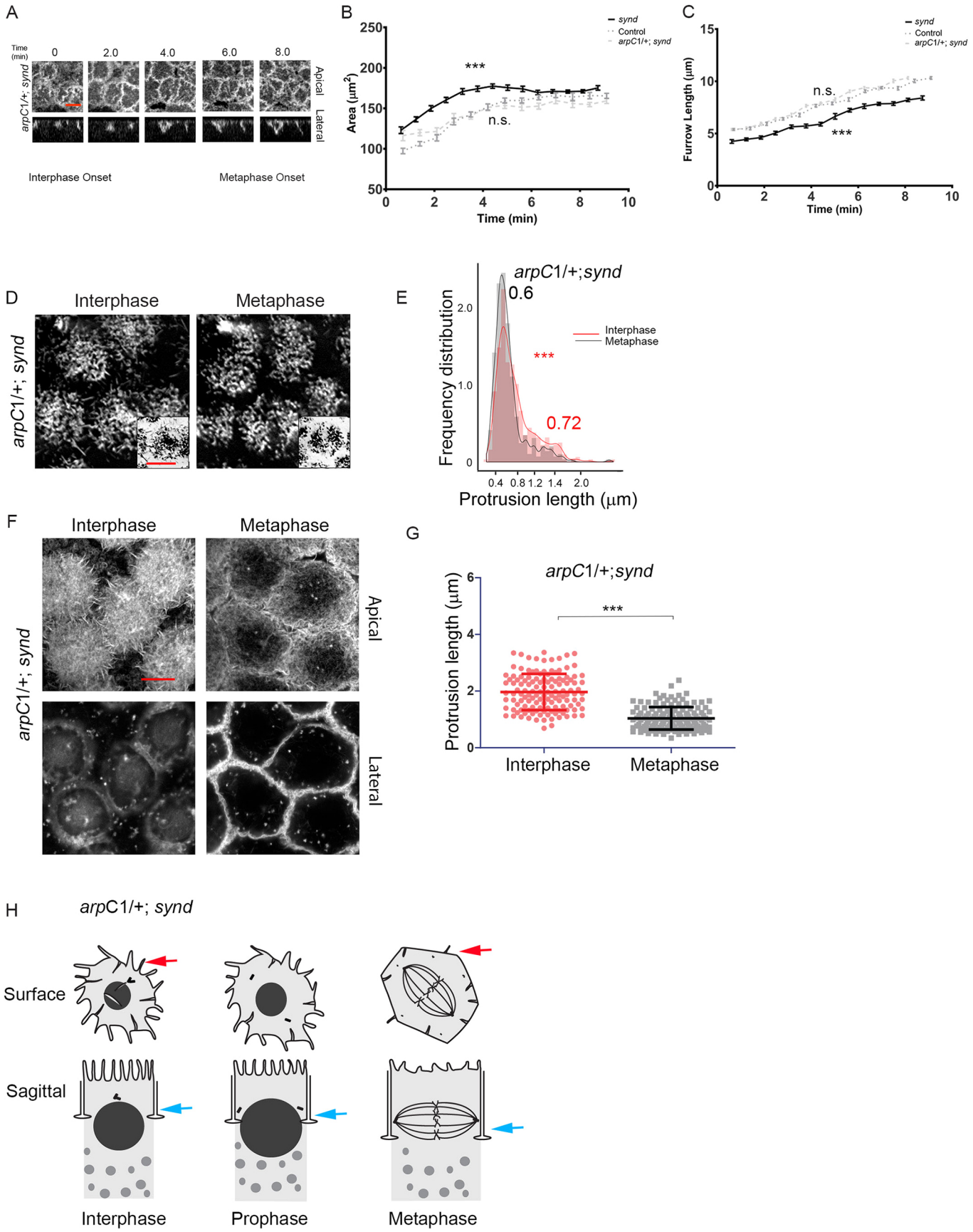

Fig. 3. See next page for legend.

Fig. 3. *arpC1/+;synd* cap and furrow dynamics are similar to controls. (A–C) Cap area (A,B) and furrow length (A,C) of *arpC1/+;synd* is comparable to that of controls (data for controls is repeated from Fig. 1B,C). Data are mean± s.e.m. of *n*=3 embryos, with three caps measured per embryo. ***P=0.001 (one-way ANOVA and Tukey's multiple comparison test). Scale bar:10 µm. (D) Apical protrusions imaged by TIRFM in NC12 *arpC1/+;synd* embryos. Scale bar: 5 µm. (E) Relative frequency distribution of protrusion lengths shows a significant difference between interphase (0.72±0.36 µm, mean±s.d.) and metaphase (0.6±0.3 µm) in *arpC1/+;synd* (***P<0.001; one-way ANOVA and Tukey's multiple comparison test) similar to controls (Fig. 2B). *n*=100 protrusions per cap, for three caps per embryo in three embryos. (F) STED microscopy of phalloidin in caps and furrows of *arpC1/+;synd* in NC12. Long protrusions are absent and furrows are present in *arpC1/+;synd* (89%, *n*=9 embryos). Scale bar: 3 µm. (G) Protrusion lengths (mean±s.d.) are significantly different between interphase and metaphase in *arpC1/+;synd*, as seen for controls, and unlike *synd* (Fig. 2D). *n*=3 embryos with ∼50 protrusions measured per embryo, ***P<0.001 (two-tailed Mann–Whitney test). (H) *arpC1/+;synd* shows decreased protrusion length and increased furrow lengths in metaphase.

Syndapin mutant phenotypes are rescued upon loss of ArpC1. Cell spreading is inhibited by low concentrations of cytochalasin D, a drug that slows the rate of actin polymerization (Wakatsuki, 2003). We have previously shown that furrow lengths are rescued when *synd* mutants are treated with low concentrations of cytochalasin D (Sherlekar and Rikhy, 2016). Here we have shown, using photobleaching experiments, that turnover of F-actin is higher in *synd* caps. Syndapin function is therefore required to limit Arp2/3 complex-mediated F-actin dynamics in the cap and to promote furrow ingression.

Myosin II is decreased in *synd* mutant caps. A theoretical model of cell spreading predicts that Myosin II in apical regions of the cell periphery facilitates spreading, whereas it opposes spreading when present in deeper regions of the lamella (Nisenholz et al., 2016). We have demonstrated that Syndapin is required to limit apical cap expansion, resulting in optimal Myosin II distribution to allow inward growth of the lateral furrow, in a manner analogous to regulation of cell spreading. Future studies on the role of Syndapin in fine tuning actin-remodeling protein activity and Myosin II-dependent contractility in different contexts will shed light on the diversity of processes that this protein can regulate in development.

MATERIALS AND METHODS

Drosophila stocks

Flies were raised on standard cornmeal agar at 25°C. Embryos from Canton S flies were used in control experiments. Homozygous escaper adults from the transposon-tagged mutant *synd*^{1d}/TM6B, Tb^{1} (Vimlesh Kumar, IISER, Bhopal, India; Kumar et al., 2009a) or adults in trans-allelic combination of *synd*^{1d}/*Df(3R)BSC43* (Bloomington stock number BL-7413) were used to generate *synd* mutant embryos. To visualize actin in apical caps we used LifeAct–GFP driven by *nanos*-Gal4 (UASp LifeAct-GFP/+; *nanos*-Gal4/+). The following lines were obtained from Bloomington Stock Center: tGPH (BL-8163), Arp3 RNAi (BL-32921), hsFLP; *arp*C1^{R337}st,neoFRT40A/CyO (BL-9136), sqh RNAi (BL-32439) and sqhGFP (BL-57145).

Immunohistochemistry

Embryos were collected for 3 h at 25°C (and at 28°C for RNAi experiments) on 3% sucrose agar plates, washed and dechorionated in 100% bleach for 1 min, fixed in equal volume of 1:1::4% PFA in PBS:Heptane for 15 min, hand/methanol devitellinized, permeabilized with 0.3% Triton-X100 in PBS (PBST), blocked with 2% BSA (Sigma-Aldrich) in PBST and immunostained with the following primary antibodies: anti-Syndapin [rat, 1:150; Vimlesh Kumar; (Kumar et al., 2009a)], anti-Arp3 [rabbit, 1:1000; William Theurkauf (University of Massachusetts Medical School, MA); (Stevenson et al., 2002)], anti-Zipper [rabbit, 1:200; Jeffrey H. Thomas (Texas Tech University Health Sciences Center, TX); (Chougule et al., 2016)], anti-Dlg [mouse, 1:10; DSHB-4F3; (Parnas et al., 2001)]. Fluorescently coupled secondary antibodies (Alexa Fluor 488, 568 and 633; Life technologies; 1:1000) were used. DNA was labeled with Hoechst 3342 (10 mg/ml; 1:1000; Life technologies) and F-actin was labeled with Alexa Fluor 488/568-conjugated phalloidin (1:100, Life technologies). The embryos were mounted in SlowFade Gold (Life technologies). Samples were imaged using a Plan-Apochromat 40×/1.3 NA oil-immersion objective on a confocal Laser Scanning Microscope (LSM 710/780, Zeiss). *z*-stacks were acquired on sequentially scanned images with a spacing of 1.08 µm between slices.

Live-embryo time-lapse imaging

Embryos were collected for 1 h, dechorionated and mounted in a LabTek chamber with PBS (Mavrakis et al., 2008) imaged in 4D (every 30 s with 0.48 or 1.08 µm between *z*-sections) by a PlanApochromat 40×/1.3 or 1.4 NA oil immersion objective on a Zeiss LSM 710/780 or a Leica SP8 inverted confocal microscope. Specific stages of the cell cycle were recognized by marking entry of fluorescent molecules in tGPH and LifeAct–GFP transgenes into the nuclear region during nuclear envelope breakdown and by observing extension of metaphase furrow length. The cap area and corresponding furrow length were measured with respect to time from interphase to metaphase transition in NC12.

Quantification of apical caps

All measurements were done on time-lapse movies of the apical caps in syncytial NC 12. Apical cap areas were measured at approximately 3 µm depth from the first visible *z* stack using the polygon tool of ImageJ (NIH, MD). The cap areas were plotted as a function of time using GraphPad Prism.

The segmented line tool in ImageJ was used to measure intensity of LifeAct–GFP along the periphery of caps as they expand. The intensity values were normalized to the maximum and plotted against time using GraphPad Prism.

Myosin II intensities with Sqh–GFP were measured in caps similar to the method used to measure LifeAct–GFP intensities. Sqh–GFP movies were taken from different genotypes under similar settings. The image corresponding to the plot at 9 min was intentionally scaled to increase brightness so that Sqh–GFP association with the cap is clearly visible in *synd* compared to control and *arpC1/+*; *synd* (Fig. 4B). Average values of Sqh–GFP were obtained from an ROI drawn at the periphery of the cap from a section at 3 µm and normalized from 0–1 (Fig. 4C). Average values of Sqh–GFP were obtained from an ROI drawn at the periphery of the cap from interphase to metaphase from a section at 3 µm (Fig. 4D). The graphs were plotted using GraphPad Prism.

TIRFM

0–1 h embryos were collected and dechorionated with 50% sodium hypochlorite. Embryos were lined up on a LabTek chamber having their ventral side facing the coverslip, in order to maximise the contact area of the embryo to the coverslip, and immersed in 1 ml PBS. Embryos were then subjected to time-lapse TIRF imaging on an Olympus Biosystems cell TIRF using an Olympus Plan APO 100× oil objective (NA 1.49). The angle of incidence was maintained at the critical angle for total internal reflection with small angular adjustments to sample illuminating angle in each experiment. In order to get optimized signals from the cortex/apical membrane, the TIRF illumination plane was set at approximately 100 nm optical section thickness from the interface. For time-lapse, images were acquired every 6 s. Post-acquisition, all time frames were deconvolved using the deconvolution algorithm provided by Olympus imaging and processing software package. TIRF images of LifeAct–GFP expressing embryos illuminated protrusions in apical caps in both interphase and metaphase. Longer protrusions were typically seen at the cap periphery and shorter protrusions were seen in the center of the cap in interphase of the syncytial cycle. The protrusions were shorter in length in metaphase. Protrusion lengths were measured manually for clearly visible and optically separable protrusions (crowded regions were omitted) (Fig. S1F) using ImageJ line tool, and their frequency distributions plotted using GraphPad Prism.

STED

Embryos were collected for 1.30–2 h at 25°C and were labeled with anti-Lamin DmO primary antibody (mouse, 1:75, AbCam) to allow observation

Journal of Cell Science (2020) 133, jcs235846. doi:10.1242/jcs.235846

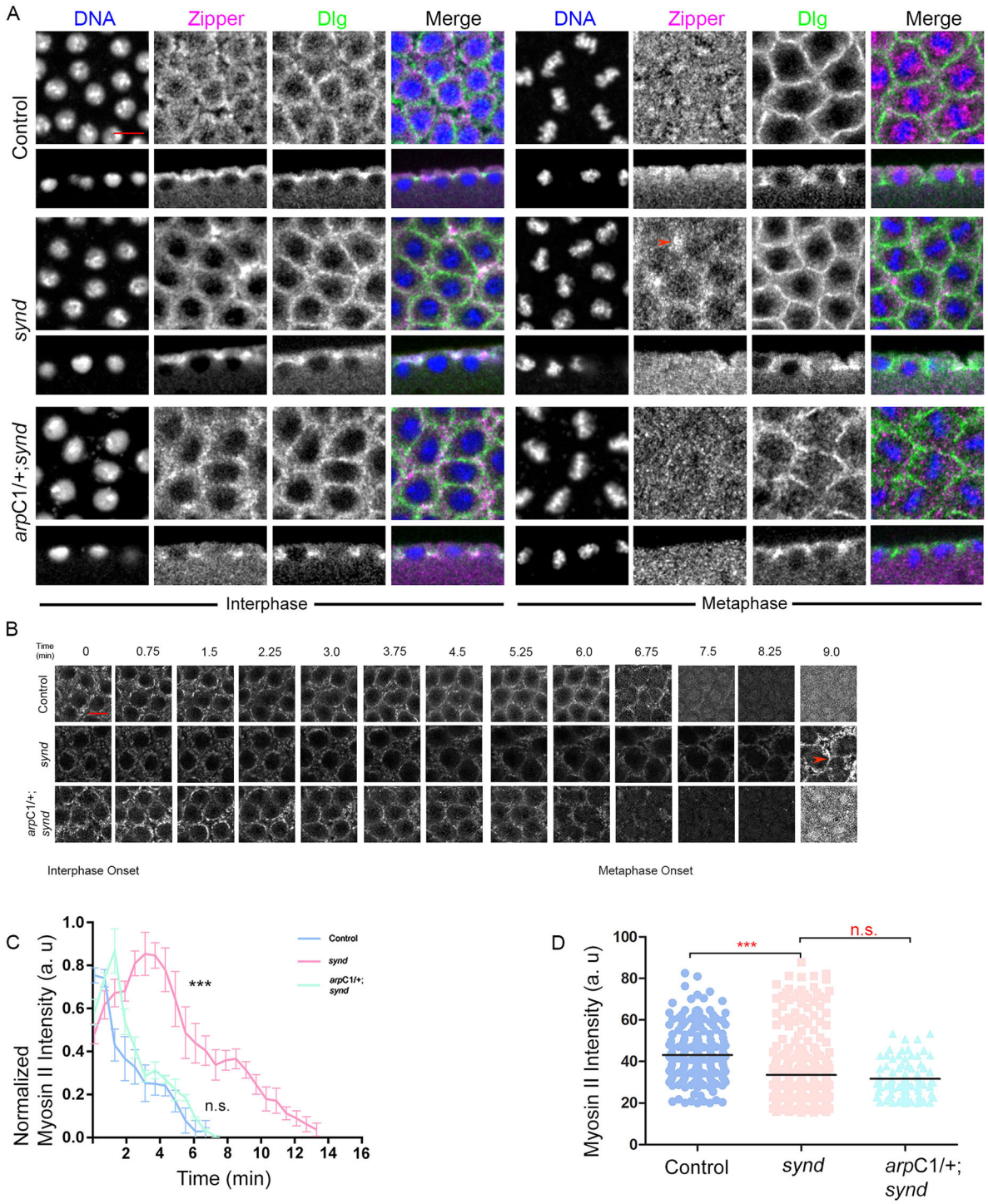

Fig. 4. Myosin II is reduced in *synd*. (A) Dlg is unaffected and Zipper is reduced and remains at tricellular junctions in *synd* (100%, *n*=15 embryos; red arrowhead) compared to control (100%, *n*=20 embryos) in metaphase, Zipper levels are rescued in *arpC*1/+;*synd* (87.5%, *n*=16 embryos). Scale bar: 10 µm. (B) Sqh–GFP in control, *synd* and *arpC*1/+;*synd*. Representative image (9 min) with increased contrast shows Sqh–GFP dissociation from the membrane in control and *arpC*1/+;*synd*, and not in *synd* (red arrowhead). Scale bar: 10 µm. (C) Relative Myosin II intensity (assayed using Sqh–GFP) versus time. Data are mean±s.e.m. of *n*=3 embryos with three caps quantified per embryo. ***P=0.001 (one-way ANOVA and Tukey's multiple comparison test). (D) Myosin II intensity (assayed using Sqh–GFP) in the indicated strains. *n*=3 embryos with three caps measured per embryo. ***P<0.001; ns, not significant (non-parametric Mann–Whitney *U*-test).

of the nucleus in order to discern the stage of the syncytial NC. This was coupled with anti-mouse Alexa Fluor 488 secondary antibody (1:1000, Life technologies). F-actin was labeled with Alexa Fluor 568 phalloidin (1:100, Life technologies). The embryo preparations were embedded in Mowiol (Sigma-Aldrich) supplemented with 2.5% DABCO (Sigma-Aldrich) to reduce fading of the fluorescence signal. All the preparations were imaged within 1–2 days to prevent loss of signal on prolonged storage.

The embryos were imaged with an inverted TCS SP8 3X microscope (Leica Microsystems, Mannheim, Germany) with a 100×/1.4 NA oil immersion (refractive index 1.518) objective (Leica HC PL APO CS2-

STED WHITE) which is operated by the Leica LAS X software (version 3.5.3). Fluorophores were excited with 488 nm (for nuclear Lamin) and 561 nm (for phalloidin) laser light derived from an 80 MHz pulsed white light laser (Leica Microsystems) at 70% intensity, and the depletion was performed with a 775 nm pulsed laser (Leica Microsystems) with a maximum power of 820–860 mW. All images were acquired in 2D STED mode, optimizing it for maximum lateral resolution improvement. The fluorophore emission was collected with Hybrid Detectors (HyD, Leica Microsystems) with a time gate of $0.8 \leq t\ g \leq 5.5$ ns with respect to the excitation pulse. A typical spectral window of 495–550 nm was used for nuclear Lamin imaging, with 570–640 nm used for phalloidin imaging. The pinhole was set to 1 AU and the images were recorded in standard mode using 5× line averaging at a zoom of 3.5× with a scan speed of 200 Hz. The images were saved and exported as 1500×1500 TIFF format images with a pixel size of about 20–25 nm.

The images were deconvolved using the STED module on Huygens Professional version 17.04 (Scientific Volume Imaging, Netherlands). To achieve maximum resolution, this software calculates the theoretical point spread function based on the given measured image and the imaging parameters from the metadata of the acquired image. For deconvolved images presented here we first estimated the average background using the In/near object module by controlling the radius parameter. Next, we used the Classical Maximum Likelihood Estimation (CMLE) algorithm by setting the maximum iterations at 40, the Signal to Noise Ratio at 7, Quality Threshold at 0.1 in the 'fast' iteration mode with possible bleaching correction. After the completion of iterations, the deconvolved images were saved as high quality TIFF images.

Phalloidin-labeled protrusions were predominantly seen at the periphery of the cap in interphase of the syncytial cycle. The most apical section was acquired in interphase and metaphase to compare the morphology. The protrusion density is reduced in metaphase of the syncytial cycle in phalloidin-labeled caps. Protrusion lengths were measured manually for clearly visible and optically separable protrusions (crowded regions were omitted) using the ImageJ segmented line tool (Fig. S1G). A scatter plot of the distribution of protrusion lengths was plotted using GraphPad Prism, with the bar representing the average and standard deviation shown.

Comparison of actin-rich protrusions from TIRFM and STED

Live embryos expressing LifeAct–GFP were used for imaging protrusions by TIRFM, and phalloidin-stained embryos were used to image protrusions by STED microscopy. Whereas LifeAct–GFP in living embryos highlighted protrusions on apical regions of caps in interphase and metaphase in TIRFM, phalloidin-labeled protrusions were enriched at the periphery in fixed embryos visualized in STED microscopy (Fig. S1F,G). The protrusions visible by TIRFM are likely to be in varied orientations. The actin filaments visible in STED images are at greater depths from the surface as compared to those visible in TIRF imaging. The longer protrusions at the periphery visible with TIRFM are likely to be the phalloidin-labeled protrusions seen in STED. Apical protrusions were not visible in STED imaging when samples were labeled with phalloidin. Faint phalloidin-labeled structures on the apical caps are bleached by the depletion laser in STED. The range of protrusion lengths seen in LifeAct–GFP-labeled embryos by TIRF followed by deconvolution is approximately 0.36 to 2.62 µm for interphase caps and approximately 0.25 to 1.46 µm for metaphase caps. The range of protrusion lengths seen in phalloidin-labeled embryos by STED followed by deconvolution is approximately 0.93 to 3.46 µm for interphase caps and approximately 0.24 to 2.52 µm for metaphase caps.

FLIP

Continuous photobleaching of the region of interest (ROI) of size 5 μm^2 was carried out on syncytial embryos expressing LifeAct–GFP using the 488 nm laser at 100% power for 30 iterations. The ROI was bleached after every second. The ROI and neighboring region were monitored for fluorescence depletion. The data was background corrected and normalized to the pre-bleach intensity, transformed on a 0–1 scale and mean intensities (a.u.) were plotted with standard error using GraphPad Prism. To represent the difference in depletion of LifeAct–GFP intensity between control and *synd* embryos, the ratio of intensities between the ROI and the neighbouring region at 50% ROI intensity depletion was plotted for control and *synd* embryos.

Acknowledgements

We thank Gaurav Diwan for help with experiments. We thank the Microscopy and *Drosophila* facilities of the Indian Institute of Science Education and Research, Pune. Stocks obtained from Bloomington *Drosophila* Stock Center (which is funded by National Institutes of Health grant P40OD018537) were used in this study.

Competing interests

The authors declare no competing or financial interests.

Author contributions

Conceptualization: A.S., R.R.; Methodology: A.S., G.M., P.R., B.D., R.R.; Formal analysis: A.S., G.M., P.R., B.D., R.R.; Investigation: A.S., G.M., P.R., B.D., S.S., R.R.; Resources: R.R.; Writing - original draft: A.S., R.R.; Writing - review & editing: A.S., B.D., R.R.; Visualization: A.S., R.R.; Supervision: R.R.; Project administration: R.R.; Funding acquisition: R.R.

Funding

A.S., B.D. and S.S. thank the Council of Scientific and Industrial Research, India for fellowships. R.R. thanks funding from the Department of Biotechnology, Ministry of Science and Technology, India (BT/PR17317/BRB/10/1521/2016), and the Indian Institute of Science Education and Research Pune.

Supplementary information

Supplementary information available online at
http://jcs.biologists.org/lookup/doi/10.1242/jcs.235846.supplemental

References

Afshar, K., Stuart, B. and Wasserman, S. A. (2000). Functional analysis of the Drosophila diaphanous FH protein in early embryonic development. *Development* **127**, 1887-1897.

Axelrod, D. (2001). Total internal reflection fluorescence microscopy in cell biology. *Traffic* **2**, 764-774. doi:10.1034/j.1600-0854.2001.21104.x

Britton, J. S., Lockwood, W. K., Li, L., Cohen, S. M. and Edgar, B. A. (2002). Drosophila's insulin/PI3-kinase pathway coordinates cellular metabolism with nutritional conditions. *Dev. Cell* **2**, 239-249. doi:10.1016/S1534-5807(02)00117-X

Cao, J., Crest, J., Fasulo, B. and Sullivan, W. (2010). Cortical actin dynamics facilitate early-stage centrosome separation. *Curr. Biol.* **20**, 770-776. doi:10.1016/j.cub.2010.02.060

Carman, P. J. and Dominguez, R. (2018). BAR domain proteins-a linkage between cellular membranes, signaling pathways, and the actin cytoskeleton. *Biophys. Rev.* **10**, 1587-1604. doi:10.1007/s12551-018-0467-7

Chougule, A. B., Hastert, M. C. and Thomas, J. H. (2016). Drak is required for actomyosin organization during Drosophila cellularization. *G3* **6**, 819-828. doi:10.1534/g3.115.026401

Dharmalingam, E., Haeckel, A., Pinyol, R., Schwintzer, L., Koch, D., Kessels, M. M. and Qualmann, B. (2009). F-BAR proteins of the syndapin family shape the plasma membrane and are crucial for neuromorphogenesis. *J Neurosci.* **29**, 13315-13327. doi:10.1523/JNEUROSCI.3973-09.2009

Fares, H., Peifer, M. and Pringle, J. R. (1995). Localization and possible functions of Drosophila septins. *Mol. Biol. Cell* **6**, 1843-1859. doi:10.1091/mbc.6.12.1843

Field, C. M. and Alberts, B. M. (1995). Anillin, a contractile ring protein that cycles from the nucleus to the cell cortex. *J. Cell Biol.* **131**, 165-178. doi:10.1083/jcb.131.1.165

Figard, L., Wang, M., Zheng, L., Golding, I. and Sokac, A. M. (2016). Membrane supply and demand regulates F-actin in a cell surface reservoir. *Dev. Cell* **37**, 267-278. doi:10.1016/j.devcel.2016.04.010

Foe, V. E. and Alberts, B. M. (1983). Studies of nuclear and cytoplasmic behaviour during the five mitotic cycles that precede gastrulation in Drosophila embryogenesis. *J. Cell Sci.* **61**, 31-70.

Foe, V. E., Field, C. M. and Odell, G. M. (2000). Microtubules and mitotic cycle phase modulate spatiotemporal distributions of F-actin and myosin II in Drosophila syncytial blastoderm embryos. *Development* **127**, 1767-1787.

Higashi, T. and Miller, A. L. (2017). Tricellular junctions: how to build junctions at the TRICkiest points of epithelial cells. *Mol Biol Cell.* **28**, 2023-2034. doi:10.1091/mbc.E16-10-0697.

Karr, T. L. and Alberts, B. M. (1986). Organization of the cytoskeleton in early Drosophila embryos. *J. Cell Biol.* **102**, 1494-1509. doi:10.1083/jcb.102.4.1494

Kessels, M. M. and Qualmann, B. (2002). Syndapins integrate N-WASP in receptor-mediated endocytosis. *EMBO J.* **21**, 6083-6094. doi:10.1093/emboj/cdf604

Kumar, V., Alla, S. R., Krishnan, K. S. and Ramaswami, M. (2009a). Syndapin is dispensable for synaptic vesicle endocytosis at the Drosophila larval

neuromuscular junction. *Mol. Cell. Neurosci.* **40**, 234-241. doi:10.1016/j.mcn.2008.10.011

Kumar, V., Fricke, R., Bhar, D., Reddy-Alla, S., Krishnan, K. S., Bogdan, S. and Ramaswami, M. (2009b). Syndapin promotes formation of a postsynaptic membrane system in Drosophila. *Mol. Biol. Cell* **20**, 2254-2264. doi:10.1091/mbc.e08-10-1072

Mavrakis, M., Rikhy, R., Lilly, M. and Lippincott-Schwartz, J. (2008). Fluorescence imaging techniques for studying Drosophila embryo development. *Curr. Protoc. Cell Biol.* **39**, 4.18.1-4.18.43. doi:10.1002/0471143030.cb0418s39

Mavrakis, M., Rikhy, R. and Lippincott-Schwartz, J. (2009). Plasma membrane polarity and compartmentalization are established before cellularization in the fly embryo. *Dev. Cell* **16**, 93-104. doi:10.1016/j.devcel.2008.11.003

Modregger, J., Ritter B., Witter, B., Paulsson, M. and Plomann, M.. (2000). All three PACSIN isoforms bind to endocytic proteins and inhibit endocytosis. *J Cell Sci.* **113**, 4511-4521.

Nisenholz, N., Paknikar, A., Köster, S. and Zemel, A. (2016). Contribution of myosin II activity to cell spreading dynamics. *Soft Mat.* **12**, 500-507. doi:10.1039/C5SM01733E

Parnas, D., Haghighi, A. P., Fetter, R. D., Kim, S. W. and Goodman, C. S. (2001). Regulation of postsynaptic structure and protein localization by the Rho-type guanine nucleotide exchange factor dPix. *Neuron* **32**, 415-424. doi:10.1016/S0896-6273(01)00485-8

Pollard, T. D. and Borisy, G. G. (2003). Cellular motility driven by assembly and disassembly of actin filaments. *Cell* **112**, 453-465. doi:10.1016/S0092-8674(03)00120-X

Ponti, A., Machacek, M., Gupton, S. L., Waterman-Storer, C. M. and Danuser, G. (2004). Two distinct actin networks drive the protrusion of migrating cells. *Science* **305**, 1782-1786. doi:10.1126/science.1100533

Royou, A., Sullivan, W. and Karess, R. (2002). Cortical recruitment of nonmuscle myosin II in early syncytial Drosophila embryos: its role in nuclear axial expansion and its regulation by Cdc2 activity. *J. Cell Biol.* **158**, 127-137. doi:10.1083/jcb.200203148

Schmidt, A. and Grosshans, J. (2018). Dynamics of cortical domains in early development. *J. Cell Sci.* **131**. doi:10.1242/jcs.212795

Sherlekar, A. and Rikhy, R. (2016). Syndapin promotes pseudocleavage furrow formation by actin organization in the syncytial Drosophila embryo. *Mol. Biol. Cell* **27**, 2064-2079. doi:10.1091/mbc.E15-09-0656

Silverman-Gavrila, R. V., Hales, K. G. and Wilde, A. (2008). Anillin-mediated targeting of peanut to pseudocleavage furrows is regulated by the GTPase ran. *Mol. Biol. Cell* **19**, 3735-3744. doi:10.1091/mbc.e08-01-0049

Sommi, P., Cheerambathur, D., Brust-Mascher, I. and Mogilner, A. (2011). Actomyosin-dependent cortical dynamics contributes to the prophase force-balance in the early Drosophila embryo. *PLoS ONE* **6**, e18366. doi:10.1371/journal.pone.0018366

Stanishneva-Konovalova, T. B., Kelley, C. F., Eskin, T. L., Messelaar, E. M., Wasserman, S. A., Sokolova, O. S. and Rodal, A. A. (2016). Coordinated autoinhibition of F-BAR domain membrane binding and WASp activation by Nervous Wreck. *Proc. Natl. Acad. Sci. USA* **113**, E5552-E5561. doi:10.1073/pnas.1524412113

Stevenson, V., Hudson, A., Cooley, L. and Theurkauf, W. E. (2002). Arp2/3-dependent pseudocleavage [correction of psuedocleavage] furrow assembly in syncytial Drosophila embryos. *Curr. Biol.* **12**, 705-711. doi:10.1016/S0960-9822(02)00807-2

Turner, F. R. and Mahowald, A. P. (1976). Scanning electron microscopy of Drosophila embryogenesis. 1. The structure of the egg envelopes and the formation of the cellular blastoderm. *Dev. Biol.* **50**, 95-108. doi:10.1016/0012-1606(76)90070-1

Wakatsuki, T. (2003). Mechanics of cell spreading: role of myosin II. *J. Cell Sci.* **116**, 1617-1625. doi:10.1242/jcs.00340

Warn, R. M., Bullard, B. and Magrath, R. (1980). Changes in the distribution of cortical myosin during the cellularization of the Drosophila embryo. *J. Embryol. Exp. Morphol.* **57**, 167-176.

Warn, R. M., Magrath, R. and Webb, S. (1984). Distribution of F-actin during cleavage of the Drosophila syncytial blastoderm. *J. Cell Biol.* **98**, 156-162. doi:10.1083/jcb.98.1.156

Webb, R. L., Rozov, O., Watkins, S. C. and McCartney, B. M. (2009). Using total internal reflection fluorescence (TIRF) microscopy to visualize cortical actin and microtubules in the Drosophila syncytial embryo. *Dev. Dyn.* **238**, 2622-2632. doi:10.1002/dvdy.22076

Young, P. E., Pesacreta, T. C. and Kiehart, D. P. (1991). Dynamic changes in the distribution of cytoplasmic myosin during Drosophila embryogenesis. *Development* **111**, 1-14.

Zallen, J. A., Cohen, Y., Hudson, A. M., Cooley, L., Wieschaus, E. and Schejter, E. D. (2002). SCAR is a primary regulator of Arp2/3-dependent morphological events in Drosophila. *J. Cell Biol.* **156**, 689-701. doi:10.1083/jcb.200109057

Zenker, J., White, M. D., Gasnier, M., Alvarez, Y. D., Lim, H. Y. G., Bissiere, S., Biro, M. and Plachta, N. (2018). Expanding actin rings zipper the mouse embryo for blastocyst formation. *Cell* **173**, 776-791.e17. doi:10.1016/j.cell.2018.02.035

Zhang, Y., Yu, J. C., Jiang, T., Fernandez-Gonzalez, R. and Harris, T. J. C. (2018). Collision of expanding actin caps with actomyosin borders for cortical bending and mitotic rounding in a syncytium. *Dev. Cell* **45**, 551-564.e4. doi:10.1016/j.devcel.2018.04.024

Supplementary Figures

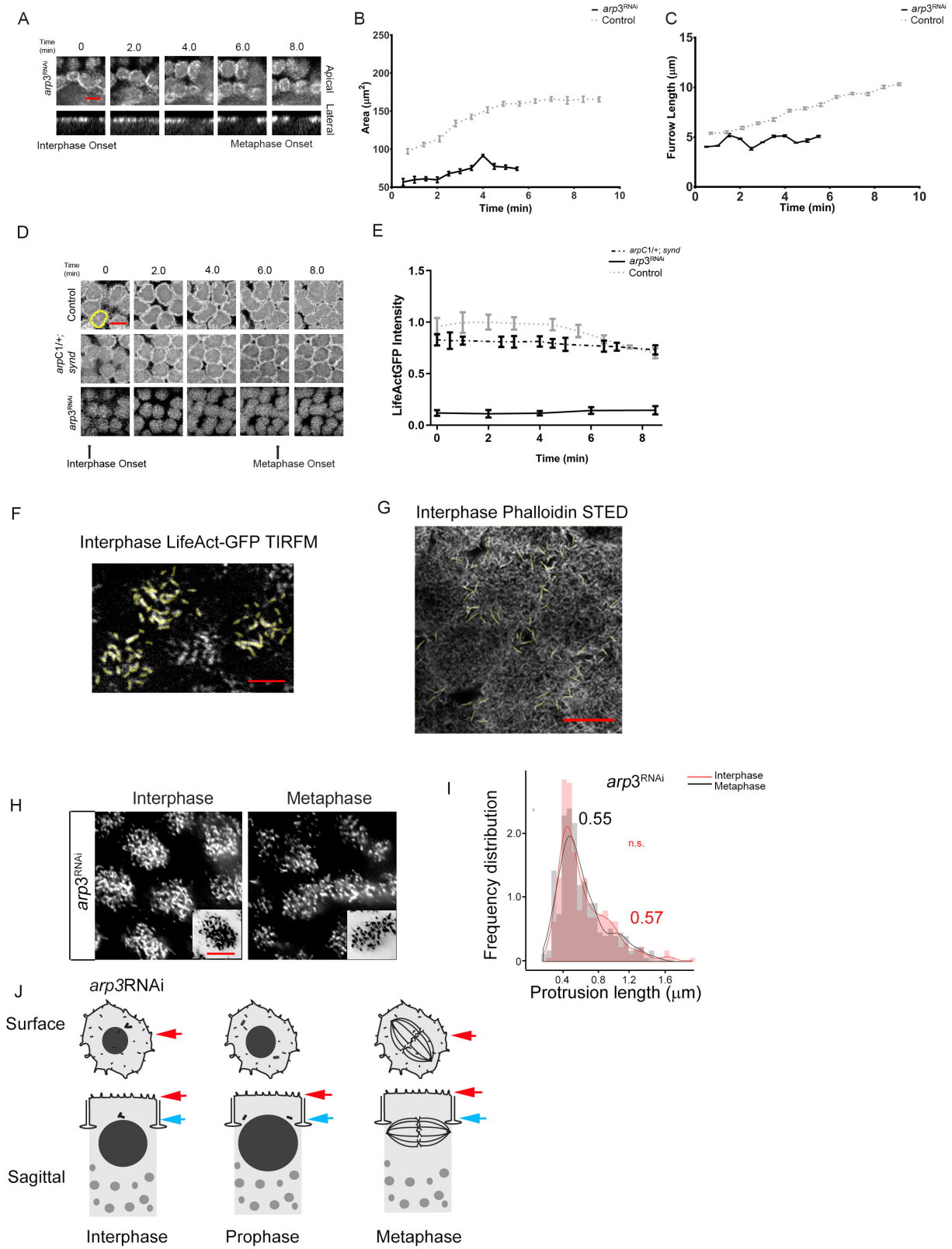

Figure S1. *arp*3^{RNAi} expressing embryos show loss of cap expansion, furrow formation and defective actin dynamics.

(A-C) Dynamics apical cap and corresponding lateral furrow extension in *arp*3^{RNAi} mutant embryos expressing tGPH (A). Graph of apical cap area for control (repeated from Figure 1B) and *arp*3^{RNAi} embryos (B) showing significantly smaller apical caps in mutant (mean ± S.E.M.; n=3; 3 caps/embryo, $p<0.01$, One-Way ANOVA and Tukey's Multiple comparison test). Graph of change in lateral furrow length in control (repeated from Figure 1C) and *arp*3^{RNAi} mutant embryos (C) (mean ± S.E.M.; n=3; 3 caps/embryo, $p<0.01$, One-Way ANOVA and Tukey's Multiple comparison test) showing significantly shorter furrows in mutant.

(D-E) LifeAct-GFP dynamics during apical cap expansion in control (repeated from Figure 1D), *arp*3^{RNAi} and *arpC*1/+;*synd* mutant embryos labeled with LifeAct-GFP (D). Graph of change in normalized LifeAct-GFP intensity vs time in control (repeated from Figure 1E), *arp*3^{RNAi} and *arpC*1/+;*synd* mutant embryos (E) (mean ± S.D.; n=3; 3 caps/embryo, One-Way ANOVA and Tukey's Multiple comparison test) showing that F-actin accumulates at the apical cap in both control and *arpC*1/+;*synd* mutant embryos ($p>0.05$), but not in *arp*3^{RNAi} mutant embryos ($p<0.01$). Scale bar=10 μm

(F-G) Sample images from LifeAct-GFP labeled embryos with TIRFM (F) and phalloidin labelled embryos with STED microscopy (G) to show optically separated objects that were quantified (yellow ROIs) in graphs shown in Figure 2 and 3 for controls, *synd* and *arpC*1/+;*synd.* Scale bar=10 μm

(H-I) Dynamics of F-actin protrusions in apical caps as revealed by TIRFM during interphase and metaphase of NC12 in *arp*3^{RNAi} mutant embryos labeled with LifeActGFP (H). Frequency distribution of protrusion lengths (I) shows smaller protrusions in interphase (0.57±0.28 µm, average±S.D. in µm) and metaphase (0.55±0.26 µm) in *arp*3^{RNAi} mutant caps (n = 100 protrusions/cap; 3 caps/embryo, 3 embryos, (n.s., p>0.05) One-Way ANOVA and Tukey's Multiple comparison test). Scale bar=10 µm

(J) Schematic showing loss of cap expansion, short protrusions and loss of furrow extension in *arp*3^{RNAi} expressing embryos.

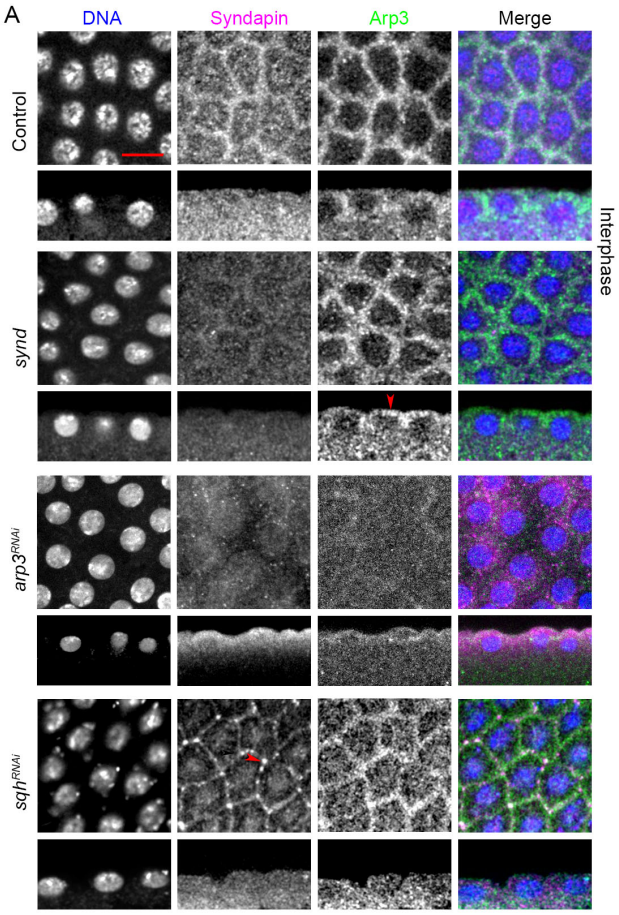

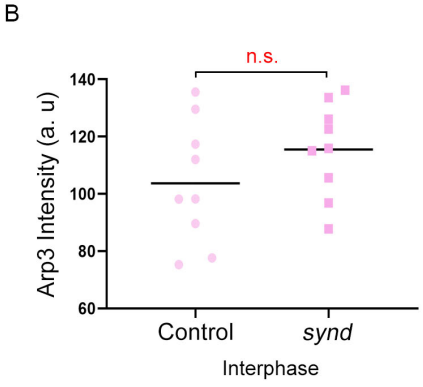

Sherlekar et al Figure S2

Figure S2. Analysis of Synd and Arp3 complex distribution in control, *synd*, *arp*3^{RNAi} and *sqh*^{RNAi} embryos.

(A) Syndapin localization to the membrane is affected in *synd* (85%, n = 60), *arp*3^{RNAi} (60%, n = 15) and *sqh*^{RNAi} embryos (100%, n = 12) red arrow indicates aberrant Syndapin localization at the membrane, particularly at tricellular junctions). Arp3 localization is spread all around the apical cortex in *synd* mutant embryos during interphase, suggesting increased Arp2/3 levels compared to control where Arp3 is enriched along the lateral furrows. Scale bar=10 μm. (B) The Arp3 intensity is plotted showing Arp3 levels in *synd* compared to control during interphase (n.s. not significant). 3 ROIs/embryo, 3 embryos, Non-parametric Mann-Whitney U test).

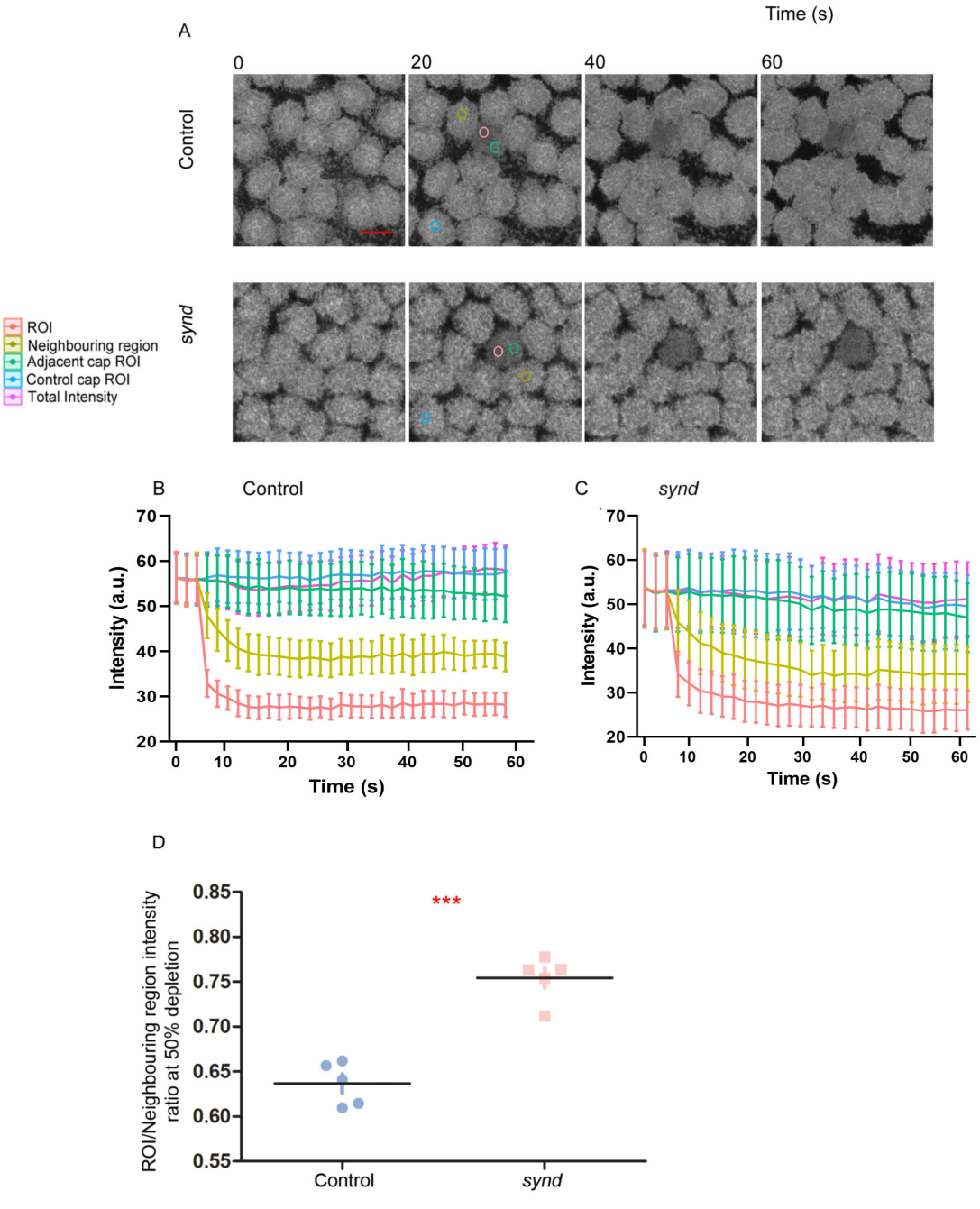

Sherlekar et al Figure S3

Figure S3. FLIP assay in apical actin caps of control and *synd* embryos.

(A) Representative time lapse images from the FLIP assay in control and *synd* mutant showing colour coded ROI bleach and control regions.

(B-C) Graph showing normalized LifeAct-GFP fluorescence intensity (Mean ± SEM) loss versus time (s) for control (B) and *synd* mutant embryos (C). Control embryos show significant difference between ROI and neighboring regions, but not *synd* embryos.

(D) Graph showing significantly different ratios of ROI and neighbor intensities at 50% depletion in control and *synd* mutant embryo caps (n=5, $p<0.001$, Non-parametric Mann-Whitney U test). Scale bar=10 μm.

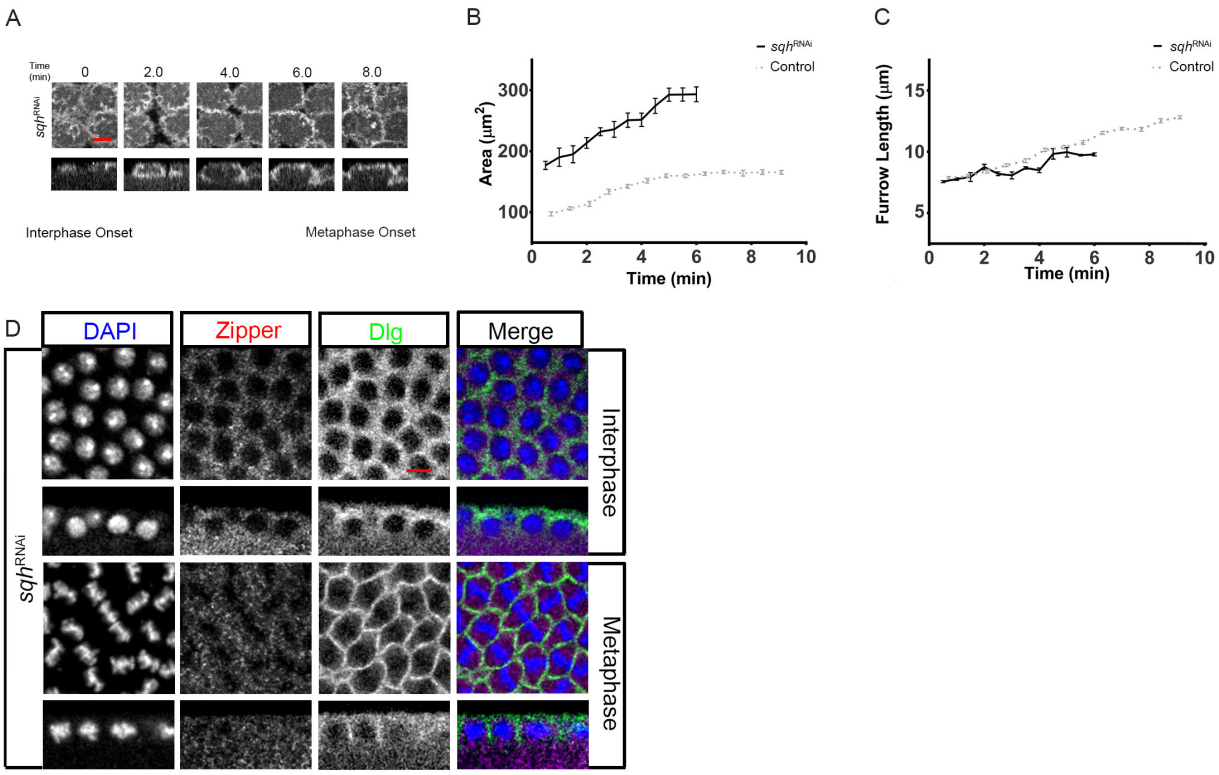

Sherlekar et al Figure S4

Figure S4. *sqh*^{RNAi} embryos show expanded cap area and shorter furrows like *synd* mutant embryos.

(A-C) Dynamics of expansion of apical cap and corresponding lateral furrow extension in control and *sqh*^{RNAi} embryos labeled with tGPH (A). Graph of change in apical cap area for control (repeated from Figure 1B) and *sqh*^{RNAi} embryos (B) showing significantly larger apical caps in mutant ($p<0.01$, mean ± S.E.M.; n=3; 3 caps/embryo, One-Way ANOVA and Tukey's Multiple comparison test). Graph of change in lateral furrow length in control and *sqh*^{RNAi} embryos (C) (mean ± S.E.M.; n=3; 3 caps/embryo, $p<0.01$, One-Way ANOVA and Tukey's Multiple comparison test) showing significantly shorter furrows in mutant.

(D) Surface and orthogonal images showing loss of Zipper (Dlg as control) localization to the membrane in interphase in *sqh*^{RNAi} embryos (66%, n = 12). Scale bar=10 μm

Supplementary Movies

All movies were acquired in four dimensions to record both cap expansion dynamics and lateral furrow extensions. Cropped movies are shown from interphase to metaphase of syncytial cycle 12. An appropriate optical section through the lateral furrow membrane in the XY plane is shown in the center showing apical caps, an orthogonal XZ section is shown at the top and an orthogonal YZ section is shown at the right for monitoring the depth of the lateral furrows. Scale bar=5 μm

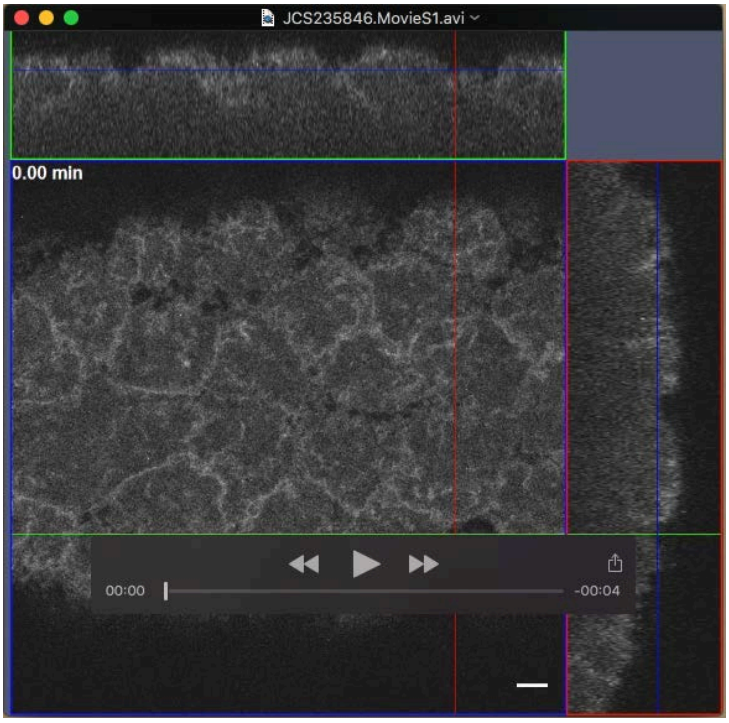

Movie 1. tGPH/+: Note the dynamics of apical cap expansion in the surface view and lateral furrow extension in orthogonal sections.

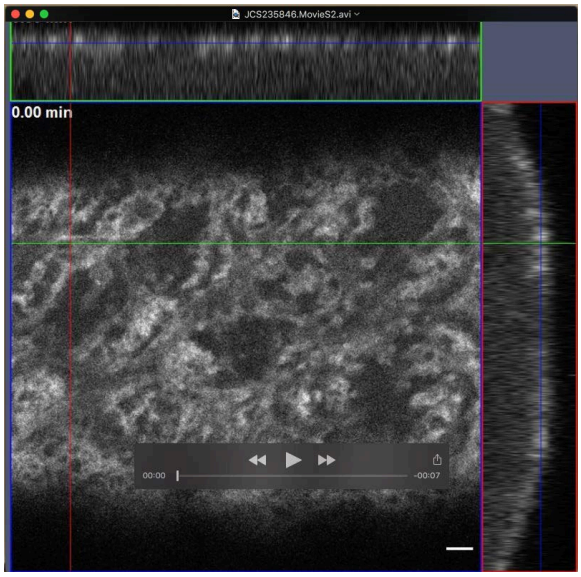

Movie 2. tGPH-*nanos*Gal4/+; *arp*3^{RNAi}: The apical caps are smaller and lateral furrows are shorter as compared to Movie 1.

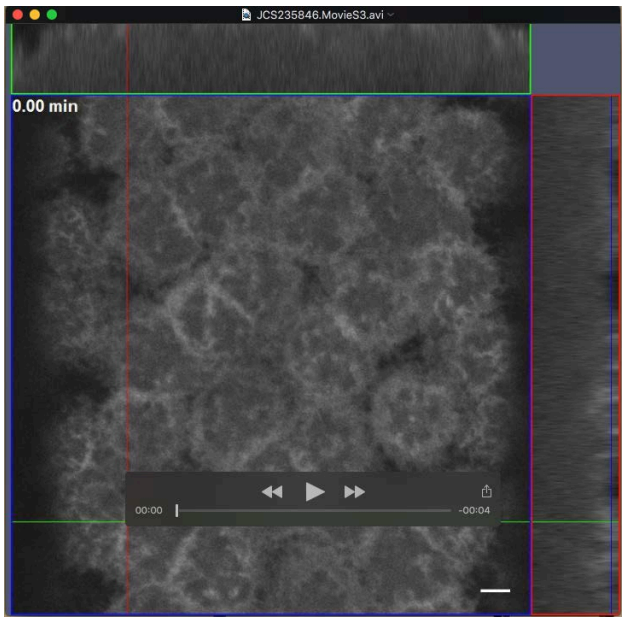

Movie 3. tGPH/+; *synd*: The apical caps are expanded whereas lateral furrow extension is lowered as compared to Movie 1.

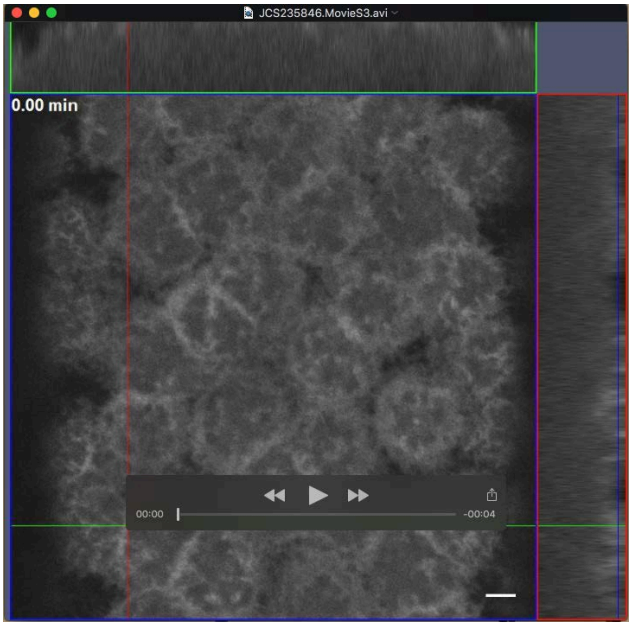

Movie 4. tGPH/*arpC*1; *synd*: The apical caps and lateral furrow extension are rescued compared to Movie 2, similar to Movie 1.

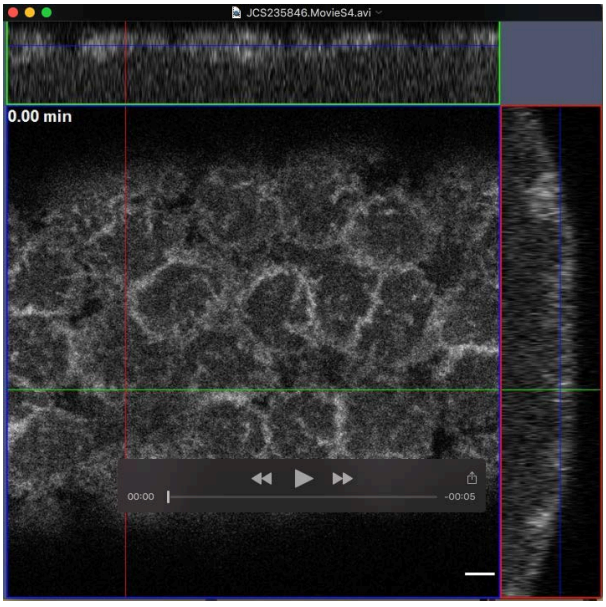

Movie 5. sqhGFP/+: Note the dynamics of Myosin II during apical cap expansion in the surface view and lateral furrow extension in orthogonal sections.

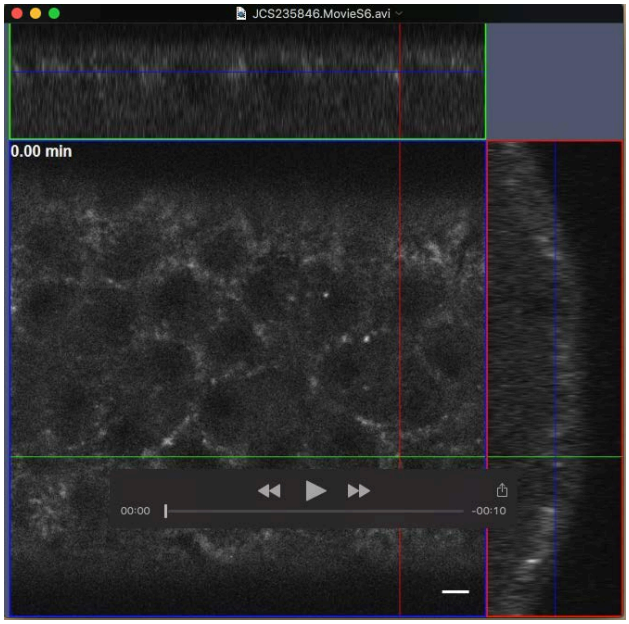

Movie 6. sqhGFP/+; *synd*: Myosin II continued to be localized at the cortex at tricellular junctions in metaphase during apical cap expansion longer than control in the surface view and lateral furrow extension in orthogonal sections.

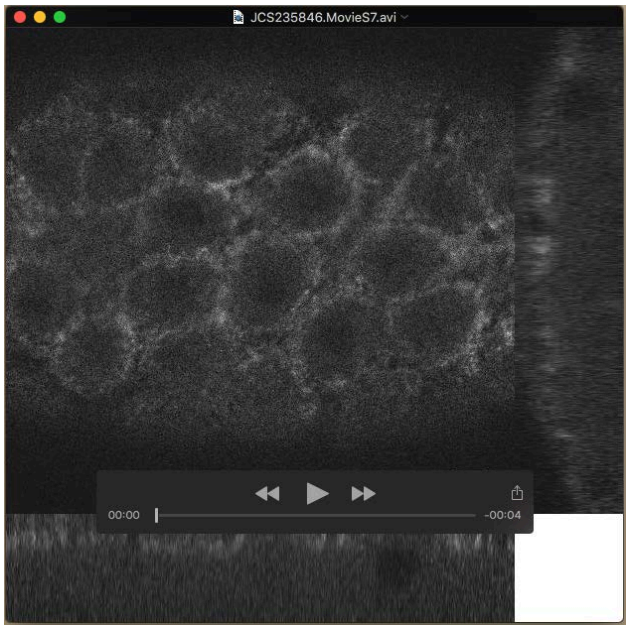

Movie 7. sqhGFP/*arpC1*; *synd*: The dynamics of Myosin II during apical cap expansion in the surface view and lateral furrow extension in orthogonal sections is similar to control.

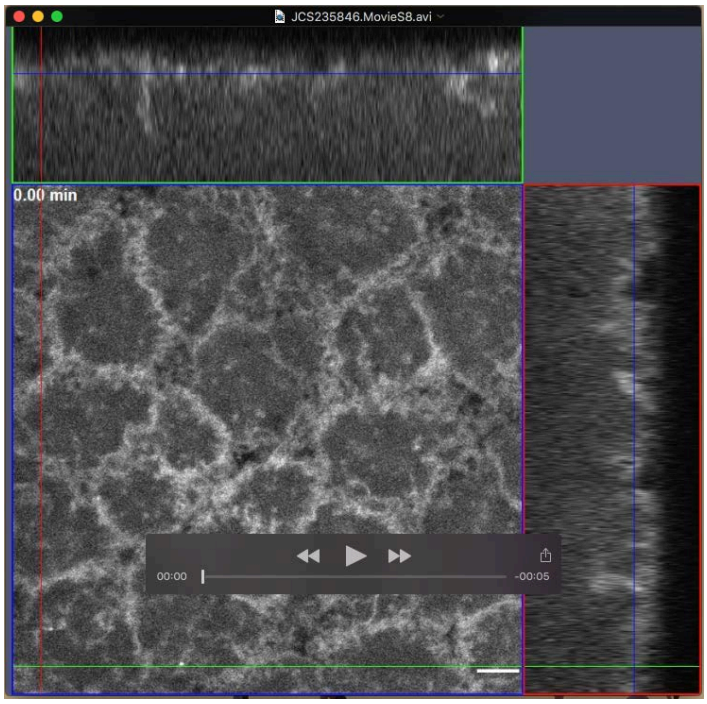

Movie 8. tGPH-nanosGal4/+; *sqh*^{RNAi}: The apical caps are expanded whereas lateral furrow extension is lowered as compared to Movie S1.